Cell models of lipid-rich α-synuclein aggregation validate known modifiers of α-synuclein biology and identify stearoyl-CoA desaturase

Thibaut Imberdis[a], Joseph Negri[a], Nagendran Ramalingam[a], Elizabeth Terry-Kantor[a], Gary P. H. Ho[a], Saranna Fanning[a], Georgia Stirtz[a], Tae-Eun Kim[a], Oren A. Levy[b], Tracy L. Young-Pearse[a], Dennis Selkoe[a], and Ulf Dettmer[a,1]

[a]Ann Romney Center for Neurologic Diseases, Department of Neurology, Brigham and Women's Hospital and Harvard Medical School, Boston, MA 02115; and [b]Department of Neurology, Columbia University Irving Medical Center, New York, NY 10032

Edited by Gregory A. Petsko, Weill Cornell Medical College, New York, NY, and approved August 29, 2019 (received for review February 27, 2019)

Microscopy of Lewy bodies in Parkinson's disease (PD) suggests they are not solely filamentous deposits of α-synuclein (αS) but also contain vesicles and other membranous material. We previously reported the existence of native αS tetramers/multimers and described engineered mutations of the αS KTKEGV repeat motifs that abrogate the multimers. The resultant excess monomers accumulate in lipid membrane-rich inclusions associated with neurotoxicity exceeding that of natural familial PD mutants, such as E46K. Here, we use the αS "3K" (E35K+E46K+E61K) engineered mutation to probe the mechanisms of reported small-molecule modifiers of αS biochemistry and then identify compounds via a medium-throughput automated screen. αS 3K, which forms round, vesicle-rich inclusions in cultured neurons and causes a PD-like, L-DOPA–responsive motor phenotype in transgenic mice, was fused to YFP, and fluorescent inclusions were quantified. Live-cell microscopy revealed the highly dynamic nature of the αS inclusions: for example, their rapid clearance by certain known modulators of αS toxicity, including tacrolimus (FK506), isradipine, nilotinib, nortriptyline, and trifluoperazine. Our automated 3K cellular screen identified inhibitors of stearoyl-CoA desaturase (SCD) that robustly prevent the αS inclusions, reduce αS 3K neurotoxicity, and prevent abnormal phosphorylation and insolubility of αS E46K. SCD inhibition restores the E46K αS multimer:monomer ratio in human neurons, and it actually increases this ratio for overexpressed wild-type αS. In accord, conditioning 3K cells in saturated fatty acids rescued, whereas unsaturated fatty acids worsened, the αS phenotypes. Our cellular screen allows probing the mechanisms of synucleinopathy and refining drug candidates, including SCD inhibitors and other lipid modulators.

Parkinson's disease | α-synuclein | multimer | neurotoxicity | therapeutic screen

The protein α-synuclein (αS), composed of 140 amino acids (aa) and highly expressed in neurons, is implicated in several neurodegenerative disorders. These "synucleinopathies" include Parkinson's disease (PD) and dementia with Lewy bodies (DLB), which have neuronal/neuritic αS-rich inclusions (Lewy bodies/neurites). In these inclusions, αS is hyper-phosphorylated at serine 129 (pS129) (1). αS has an 11-aa repeat motif with the core consensus sequence KTKEGV that appears imperfectly 6 to 9 times in the first two thirds of the protein (2). αS missense mutations such as E46K lead to rare, aggressive forms of familial PD (fPD) and DLB (3), but excess wild-type (WT) αS can also cause synucleinopathy (e.g., via gene triplication) (4).

Recent data suggest that Lewy-type inclusions are rich in lipids/membranes and thus not principally fibrillar as previously thought (5). Lipid-related risk genes have emerged from genetic studies, most importantly glucocerebrosidase A (*GBA*, GCase), a key enzyme in glycolipid catabolism proposed to form a "bidirectional pathogenic loop" with αS (6). GCase functional deficiency leads to αS dyshomeostasis, including a lack of native multimerization. Inhibiting glycolipid anabolism via the compound miglustat restores metastable physiological αS multimerization (7), which can be trapped in situ by live-cell cross-linking and Western blot (WB) (8–10). Transient lipid association has been implicated in αS multimer assembly (11). αS binding to small vesicles is well-documented in vitro and mediated by the formation of transient αS amphipathic helices at highly curved membranes (12–14). These helices are promoted by hydrophobic aa that interact with the fatty acyl chains of membrane lipids and by lysine residues that interact with negatively charged phospholipid head groups (15). The additional lysine in fPD-linked αS E46K was proposed to stabilize the monomeric, membrane-associated helix of αS (16).

Current therapeutics for synucleinopathies are symptomatic, not disease-modifying. PD and DLB are complex disorders involving multiple factors and develop over many years of protein dyshomeostasis. There is a need for cellular models that exhibit phenotypes on an accelerated timeline: synucleinopathies develop in brains over decades, yet cellular research and screens require robust phenotypes within days. Here, we propose such an "accelerated" model that expresses YFP-tagged αS "3K" (αS-3K::YFP) in human neuroblastoma cells. In αS 3K (E35K+E46K+E61K), the fPD E46K mutation has been "amplified" by inserting analogous mutations into the immediately adjacent KTKEGV repeat motifs. In cell culture, αS

Significance

Misfolding and accumulation of the protein α-synudein (αS) inside nerve cells characterize Parkinson's disease (PD) and related brain diseases, for which no disease-modifying therapies exist. Robust cell models are needed that recapitulate abnormal αS folding/accumulation in real time, especially for compound screening. We took advantage of the engineered αS "3K" (E35K+E46K+E61K) mutation, which amplifies the familial PD-causing E46K and readily forms round inclusions. We rescued the inclusions with known αS modulators and then screened a ∼2,000-compound library. We identified the potential therapeutic target stearoyl-CoA desaturase; its inhibition cleared αS inclusions, in accord with the effects of conditioning in saturated fatty acids. We propose a model for how fatty acids serve as key modulators of cellular αS homeostasis.

Author contributions: T.I., J.N., D.S., and U.D. designed research; T.I., J.N., E.T.-K., G.S., T.-E.K., and U.D. performed research; T.I., J.N., N.R., G.P.H.H., S.F., O.A.L., T.L.Y.-P., and U.D. contributed new reagents/analytic tools; T.I., J.N., E.T.-K., and U.D. analyzed data; and T.I., J.N., E.T.-K., D.S., and U.D. wrote the paper.

Conflict of interest statement: D.S. is a director and consultant to Prothena Biosciences.

This article is a PNAS Direct Submission.

[1]To whom correspondence may be addressed. Email: udettmer@bwh.harvard.edu.

This article contains supporting information online at www.pnas.org/lookup/suppl/doi:10.1073/pnas.1903216116/-/DCSupplemental.

First Published September 23, 2019.

3K exhibits multiple biochemical and cytopathological changes resembling features of PD, most importantly lipid/membrane-rich αS aggregation (17) that is consistent with a recent characterization of Lewy bodies (5). In a mouse model, the pan-neuronal expression of αS 3K causes an L-DOPA–responsive motor phenotype closely resembling PD (18). Here, we propose that a cellular model expressing αS 3K::YFP can be leveraged to screen drugs and probe into their mechanisms. First, we showed that published modifiers of αS dyshomeostasis/toxicity such as isradipine (19), nilotinib (20), fingolimod (21), nortriptyline (22), and trifluoperazine (23) can reduce αS 3K::YFP inclusions. Differences in the observed kinetics shed further light on their mechanisms. Next, we screened a library of 1,902 compounds for their ability to lower αS inclusion burden. The most compelling hits emerging from this screen were inhibitors of stearoyl-CoA desaturase (SCD), the rate-limiting enzyme for conversion of saturated to monounsaturated fatty acids (FAs). SCD inhibitors ameliorated several PD-relevant biochemical alterations in αS and decreased αS-mediated cytotoxicity. Based on these findings, we propose a model for the complex relationship between αS, lipids, and membranes in which lowering monounsaturated FAs can ameliorate pathological changes in αS biology.

Results

αS 3K Mutant and Its Cytoplasmic Inclusion Formation. The fPD-linked mutant E46K changes the αS repeat core motif KTKEGV to KTKKGV in repeat 4 (Fig. 1*A*), stabilizing membrane-associated helical αS (16). When fused to YFP and expressed in neuroblastoma cells, αS E46K, compound mutant "2K" (E35K+E46K; repeats 3+4), and compound mutant "3K" (E35K+E46K+E61K; repeats 3+4+5) exhibit stepwise increases in inclusion formation relative to wt (Fig. 1*A*). The inclusions can be visualized in live cells by fluorescence microscopy and are typically infrequent and small for αS E46K, more pronounced for 2K, and easily detectable for αS 3K (Fig. 1*A* and *SI Appendix*, Fig. S1). Similar stepwise changes toward pathology-relevant phenotypes have been observed for 1K–3K with regard to solubility (decrease), native multimerization (decrease), and toxicity (increase) (24). These stepwise effects in cell culture, biophysical data (25), and findings from the αS 3K mouse model (18) (summarized in *SI Appendix*, Table S1) indicated to us that αS 3K models synucleinopathy-relevant phenotypes and might be exploited as a discovery model (followed by validation in fPD and wt αS excess models). To take advantage of the pronounced 3K::YFP inclusion phenotype while avoiding continuous toxicity, we generated doxycycline (dox)-inducible M17D neuroblastoma cells (M17D/αS-3K::YFP). Constitutive coexpression of mCherry RFP allowed us to assess toxic effects and to normalize inclusions to cell numbers. At 12 h post induction, YFP was visible and first inclusions appeared (Fig. 1*B* and *SI Appendix*, Fig. S2). At 24 h, many cells contained inclusions, which electron microscopy (EM) identified as medleys of lipid droplets (LDs), vesicles/membranes (arrows), and αS (Fig. 1 *B*, *Top Right*; *SI Appendix*, Fig. S3 shows detailed EM images of additional examples of such lipid-rich inclusions, plus αS immunogold staining), consistent with our previous observations (17) and with recent insight into Lewy body structure (5). Fluorescence and bright-field images were acquired in the IncuCyte system (Essen), which also provided unbiased automated image analyses.

Known αS-Relevant Compounds Reduce αS 3K Inclusions. Given the lipid nature of our αS inclusions and the PD relevance of the lipid-related genetic risk factor *GBA*/GCAse, we tested the drug miglustat in our assay. Miglustat has been described to improve αS folding homeostasis in the case of GCase deficiency (7). M17D/αS-3K::YFP cultures were pretreated with miglustat or DMSO vehicle for 24 h prior to dox induction. At 24 h post dox treatment, cultures were analyzed. Cells treated with DMSO vehicle developed numerous punctate αS-3K::YFP signals (Fig. 2*B*). Nontoxic (Fig. 2*A*) concentrations of miglustat (25 μM) decreased cellular inclusion burden by ~25% (Fig. 2*B*) without affecting αS levels (Fig. 2*C*). Next, using the same paradigm, we analyzed further compounds reported to rescue αS abnormalities in earlier wt and fPD cellular and/or rodent models. Cells treated with DMSO vehicle again developed numerous αS-3K::YFP puncta (Fig. 2*D*), while cells pretreated with 5 μM trifluoperazine (TFP) (23) developed fewer inclusions, and 10 μM TFP nearly abolished them (Fig. 2*D* and *SI Appendix*, Fig. S4). TFP and a second known αS-modifying compound, nortriptyline (NOR) (22), each showed dose-dependent inclusion lowering, and their IC_{50} values in this prevention paradigm were 2.75 ± 0.32 μM and 6.18 ± 1.63 μM, respectively (Fig. 2*D*). Both TFP and NOR decreased αS pS129 levels in both cell lines expressing αS 3K (*SI Appendix*, Fig. S5*A*) and αS E46K (*SI Appendix*, Fig. S5*B*). Additional compounds reported to affect αS such as fingolimod (21), FK506 (26), isradipine (19), nilotinib (20), squalamine

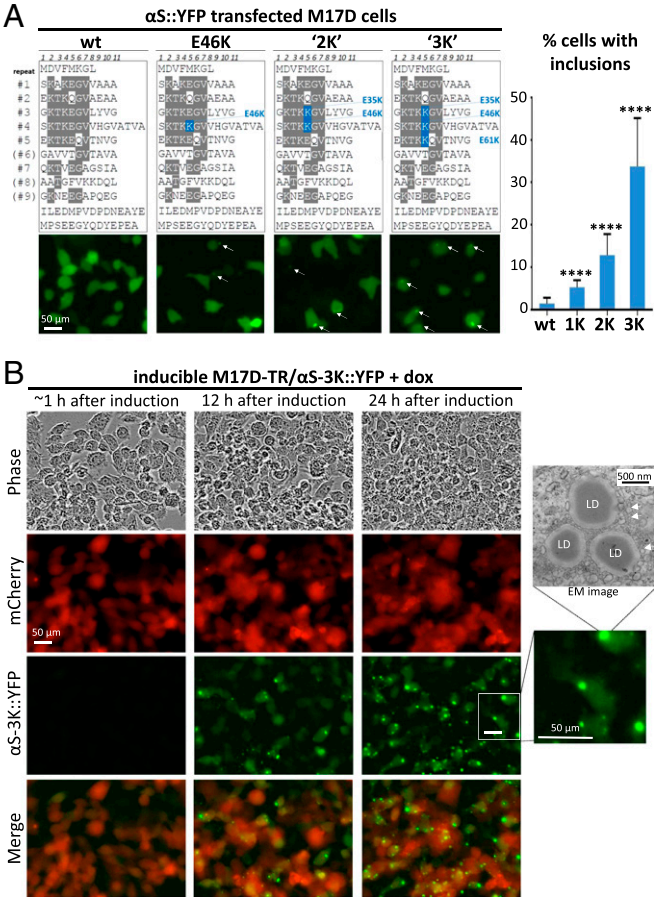

Fig. 1. αS inclusion formation in M17D neuroblastoma cells. (*A*) The indicated αS variants (aligned by KTKEGV motifs; *Top*) were transiently expressed as YFP fusion proteins in M17D cells and studied by fluorescence microscopy of live cells after 24 h (*Bottom*). (*Right*) Cells +/– inclusions were counted in a blinded fashion (100 cells per well; 3 independent experiments with 8 wells per variant; $n = 24$). *SI Appendix*, Fig. S1 shows cellular context, cotransfected RFP, and bright-field images. (*B*) Inducible αS-3K::YFP-expressing cells. M17D cells expressing constitutive mCherry and dox-inducible αS-3K::YFP were induced for 24 h. Images were taken every 2 h (phase, red, green). At 12 h after induction, αS-3K::YFP and first inclusions became visible. At 24 h, many round cytoplasmic inclusions were detected. (*Top Right*) Electron microscopy of an M17D-TR/aS-3K::YFP inclusion. Arrows point at vesicular structures in the inclusions. LD, nearby lipid droplet-like structures. Fluorescent images represent >20 independent experiments; EM images >5. Scale bars as indicated. Graphs are means ± SD. Criteria for significance relative to untreated wt was ****$P < 0.0001$.

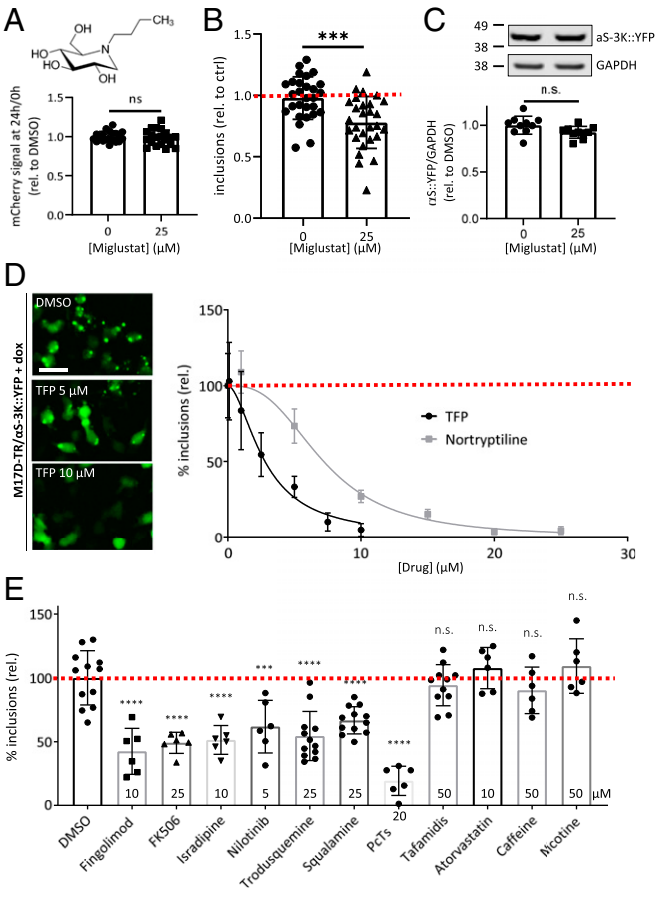

Fig. 2. Previously reported PD drug candidates rescue αS inclusions. (*A*, *Top*) Structure of miglustat (Fisher Scientific, ref. 31-171-0); (*A*, *Bottom*) Cells treated with 25 μM miglustat for 24 h and then induced for 24 h; growth rates (mCherry signals 24 h vs. 0 h after induction) relative to DMSO control ($n = 10$). (*B*) Same treatments as in *A*; inclusions 24 h after induction (normalized to mCherry; percentage of DMSO vehicle; $n = 28$). (*C*) Same treatments as in *A*; representative WB and quantification of αS-3K::YFP and GAPDH loading control ($n = 10$). (*D*, *Left*) Inducible M17D-TR/αS-3K::YFP cells were treated for 24 h with trifluoperazine (TFP) at 5 μM or 10 μM or DMSO vehicle control, and then inclusions were followed over 24 h. Representative images. (Scale bar, 50 μm.) (*D*, *Right*) Dose response of TFP and nortriptyline (NOR): inclusion quantification (normalized to constitutive mCherry and expressed as a percentage of DMSO vehicle control); $n = 12$ for DMSO and $n = 6$ for each drug concentration. (*E*) Cells treated for 24 h with nontoxic concentrations of fingolimod (10 μM), FK506 (25 μM), isradipine (10 μM), nilotinib (5 μM), trodusquemine (25 μM), squalamine (25 μM), phthalocyanine tetrasulfonate (PcTs; 20 μM), tafamidis (50 μM), atorvastatin (10 μM), caffeine (50 μM), or nicotine (50 μM). Cells were induced 24 h after treatment, and inclusions were quantified 24 h after induction (normalized to mCherry; percentage of DMSO vehicle); $n = 12$ for DMSO, trodusquemine, squalamine, and tafamidis; $n = 6$ for all others. Graphs are means ± SD. Criteria for significance relative to DMSO vehicle were ***$P < 0.001$ and ****$P < 0.0001$; n.s., not significant.

(27), trodusquemine (28), and phthalocyanine tetrasulfonate (PcTs) (29) also decreased inclusion burden (Fig. 2*E* and *SI Appendix*, Fig. S4) at noncytotoxic concentrations (*SI Appendix*, Fig. S6*A*). Interestingly, caffeine and nicotine, which may be linked to reduced PD risk in epidemiological studies (30), did not noticeably prevent αS 3K inclusions (Fig. 2*E*). Statins have been associated with both reduced (e.g., ref. 31) and increased (e.g., ref. 32) PD risk, but atorvastatin did not affect our model. Last, the unrelated drug tafamidis, designed to stabilize transthyretin tetramers (33), did not have effects. These negative results underscore the specificity of our assay. To assess whether the effect of the positive drugs might be due to altered αS levels, we performed WB (*SI Appendix*, Fig. S6 *B* and *C*). At $n = 9$, no drug significantly altered total αS levels, suggesting that the active compounds act primarily via αS redistribution. We also confirmed that none of the drugs artificially affected YFP fluorescence, e.g., by emitting at the same wavelength (*SI Appendix*, Fig. S7).

Next, we asked if these compounds were capable of ameliorating existing inclusions in a rescue paradigm. αS-3K::YFP expression was dox-induced for 24 h and then compound treatment was initiated. Inclusions were quantified 1 h and 24 h after initiation of treatment relative to DMSO vehicle alone. TFP, NOR, fingolimod, FK506, nilotinib, and PcTs each lowered inclusion-integrated intensities within 1 h after initiating treatment (Fig. 3). Among these compounds, TFP and NOR showed the strongest effects, with the majority of inclusions abrogated within 1 h at the highest treatment concentrations (10 μM TFP; 25 μM NOR). Isradipine did not significantly rescue preexisting inclusions acutely (1 h), only after 24 h, while squalamine and trodusquemine showed no effects (Fig. 3*B*). Because TFP exhibited the most rapid and potent effect (IC_{50} ~5 μM), we examined its action in a time-series experiment. Following a 24-h induction of αS-3K::YFP expression, cultures were treated with 10 μM TFP and imaged at 5-s intervals over 5 min.

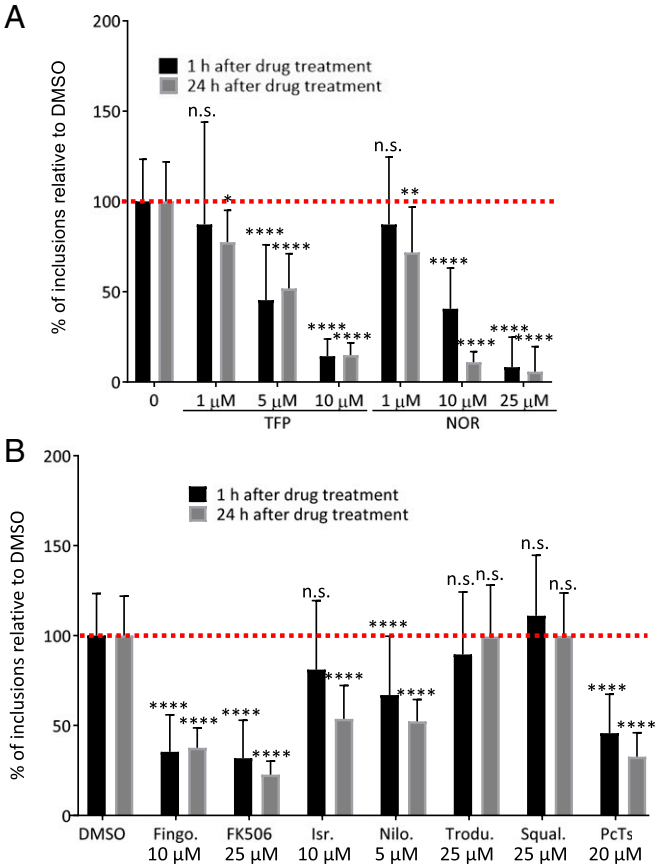

Fig. 3. Previously reported PD drug candidates dissolve αS inclusions at different kinetics. (*A*) M17D-TR/αS-3K::YFP cells dox-induced for 24 h and then treated with 1, 5, or 10 μM TFP or 1, 10, or 25 μM NOR. Inclusions quantified at the 1-h first read (black bars) or 24 h after treatment (gray bars), normalized to constitutive mCherry, expressed as percentage of DMSO control at the same time point ($n = 24$). (*B*) Analogous to *A*; cells treated with nontoxic concentrations of fingolimod (10 μM), FK506 (25 μM), isradipine (10 μM), nilotinib (5 μM), trodusquemine (25 μM), squalamine (25 μM), or PcTs (20 μM); $n = 24$. Graphs are means ± SD. Criteria for significance relative to DMSO vehicle were *$P < 0.05$, **$P < 0.01$, and ****$P < 0.0001$; n.s., not significant.

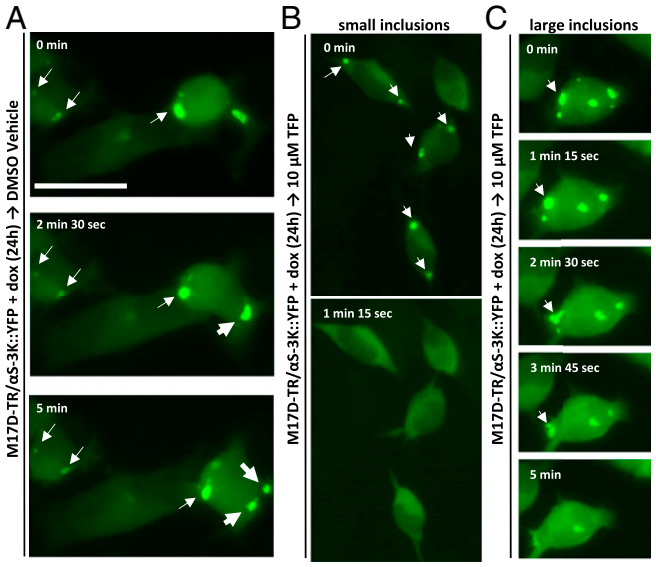

Fig. 4. TFP rapidly rescues existing inclusions. After induction for 24 h, M17D-TR/αS-3K::YFP cells were treated with 10 μM TFP and imaged every 5 s. Arrows point at inclusions. (*A*) DMSO vehicle control did not reduce preformed inclusions within 5 min (thick arrow points at an inclusion that undergoes fission, underlining the dynamic nature of the inclusions). (*B*) Small inclusions were typically dissolved between 1 and 2 min after treatment. (*C*) Bigger inclusions were dissolved within ∼5 min. (Scale bar, 50 μm.)

Most of the smaller inclusions (≤2-μm diameter) dissociated within 1 to 2 min (Fig. 4*B*), whereas larger ones (≥4-μm diameter) typically required 5 min to dissolve completely (Fig. 4*C* and Movie S2). The vehicle control DMSO did not dissociate preformed inclusions as expected (Fig. 4*A* and Movie S1), but changes in their morphology over time (Fig. 4*A*, thin arrows) or even splitting events (Fig. 4*A*, thick arrow) underline the dynamic nature of the inclusions, as published before (17).

High-Content Screening of a Bioactive Compound Library. Based on the consistent effects of several known compounds both in rescuing αS phenotypes in other models and rescuing our αS-3K::YFP inclusion phenotype, we concluded that the latter assay represents a relevant cellular model of αS dyshomeostasis. To identify novel druggable targets that can mitigate αS inclusion formation, we performed a high-content screen of an annotated bioactive library of 1,902 small compounds (Selleck) in duplicate at a 10-μM final concentration (*SI Appendix*, Fig. S8). To that end, the assay was miniaturized to a 384-well plate format. The protocol involved simultaneous induction of αS-3K::YFP expression and treatment. After 24 h, αS-3K::YFP inclusion and nuclei counts in each well were quantified with a custom CellProfiler (34) protocol. Statistics were calculated using custom scripts in R (35). The degree of lowering of αS-3K::YFP inclusion number was expressed as a percentage determined by 2-point normalization against DMSO-negative (100%) and TFP-(10 μM) positive control (0%). Compounds that induced cytotoxicity, as determined by a count of Hoechst-stained nuclei >2 SD below the mean of the DMSO control, were excluded from further analysis. Z' scores determined in prescreen test experiments were routinely >0.5. In the actual screen that was performed on several different days, the Z' value across the plates had a median of 0.27 (−0.01 to 0.45 IQR), indicating a suitable high-content assay. Fourteen compounds reduced inclusions by >75%, another 74 compounds by >50%, and another 432 compounds by >25%; all those compounds were considered primary hits. Pathway analyses led us to consider receptor tyrosine kinases (c-kit, c-met, VEGFR), autophagy, calcium signaling, and lipid/FA pathways. We pursued the lipid-related hits further because of 1) EM analyses (Fig. 1 and ref. 17) suggesting membrane and neutral lipids to be a major component of αS 3K inclusions, 2) the lipid nature of Lewy bodies (5), 3) the relative novelty vs. autophagy or calcium signaling, and 4) the lack of neuronal relevance of c-kit/c-met/VEGFR signaling. Among the lipid-related hits, relevant inclusion prevention was observed for inhibitors of cyclooxygenase (23 hits of 48), HMG-CoA reductase (3/9), phospholipase A (3/9), PI3-kinase (3/18), FA amide hydrolase (3/4), lipases (3/4), and stearoyl-CoA reductase (SCD; 2/2). We settled on pursuing SCD, the enzyme that catalyzes the formation of monounsaturated FAs (MUFAs) from saturated FAs (SFAs) because 1) our group has a longstanding interest in the relevance of lipid saturation on αS homeostasis (36); 2) earlier findings of Lindquist and colleagues on the upregulation of the MUFA oleic acid (OA) in αS-expressing yeast, leading to the intriguing hypothesis that OA in turn may affect αS biology; and 3) the αS literature documenting the importance of membrane lipid composition in synucleinopathies (e.g., refs. 37 and 38).

SCD, a Target that Modulates αS Inclusions: Proof of Concept. The 2 SCD inhibitors identified in the primary screen, PluriSln1 and MK-8245, were retested using fresh compound. When cultures were pretreated 24 h prior to αS-3K::YFP induction, 10 μM PluriSln1 and 10 μM MK-8245 reduced inclusions by 85% and 45%, respectively, vs. DMSO vehicle (Fig. 5*A* and *SI Appendix*, Fig. S6*D*). WB of cell lysates confirmed similar levels of αS-3K::YFP (*SI Appendix*, Fig. S6 *E* and *F*). To further validate SCD as a bona fide target for modulating αS homeostasis, 3 additional commercially available SCD inhibitors, A939572, CAY10566, and MF-438, were examined. All 3 exhibited higher potency than the most potent hit from the screen. IC_{50} of CAY10566 was 0.15 ± 0.09 μM, that of A939572 was 0.45 ± 0.75 μM, and that of MF-438 was 0.72 ± 0.53 μM, vs. that of PluriSln1, 3.01 ± 2.09 μM (Fig. 5*B*). A939572 significantly increased levels of αS-3K::YFP by WB whereas CAY10566 trended toward decreasing it (P value 0.06; n = 9). These opposite effects and their absence for other SCD inhibitors suggested that inclusion formation is not primarily altered via αS levels (*SI Appendix*, Fig. S6 *E* and *F*). None of the SCD inhibitors was toxic at 10 μM (*SI Appendix*, Fig. S6*D*).

We then tested effects on preexisting inclusions. Cells were induced 24 h prior to initiating treatment with 1, 5, or 10 μM of CAY10566, and then inclusions were monitored for a further 24 h. Following 1 h exposure to CAY10566, there was a significant decrease in inclusions at the higher dose (10 μM), whereas after 24 h exposure we observed a dose-dependent reduction across all 3 concentrations tested (Fig. 5*C*). Next, SCD1 expression was targeted using DsiRNA knockdown. We used 3 separate oligos: no. 3 for the exon 5 coding sequence and nos. 5 and 7 for the 3′ UTR of exon 6. Compared to scrambled DsiRNA and mock transfection, all 3 oligos decreased inclusion formation, and so did the pooled oligos (Fig. 5*D*). We confirmed SCD1 knockdown and similar αS-3K::YFP levels by WB (Fig. 5*E*); the degree of rescue of the inclusion phenotype correlated with the extent of knockdown of SCD1 expression (Fig. 5*E*).

SCD Inhibitors Affect αS Homeostasis and Toxicity in Neuronal Cells. We next tested the effects of SCD inhibition on relevant aspects of cellular αS dyshomeostasis. First, shifts to abnormally low αS multimer:monomer (αS60:14) ratios have been observed in the context of genetic forms of synucleinopathies, including αS fPD mutants (24) and the glucocerebrosidase-A form of PD (7). Second, increased phosphorylation of αS at Serine129 (pS129) is a known marker of αS dyshomeostasis in PD and models thereof (1). CAY10566 treatment (10 μM) of M17D/αS-3K cells for 48 h markedly increased αS60:14 ratios, while unchanged dimer:monomer ratios of endogenous DJ-1 confirmed equal cross-linking

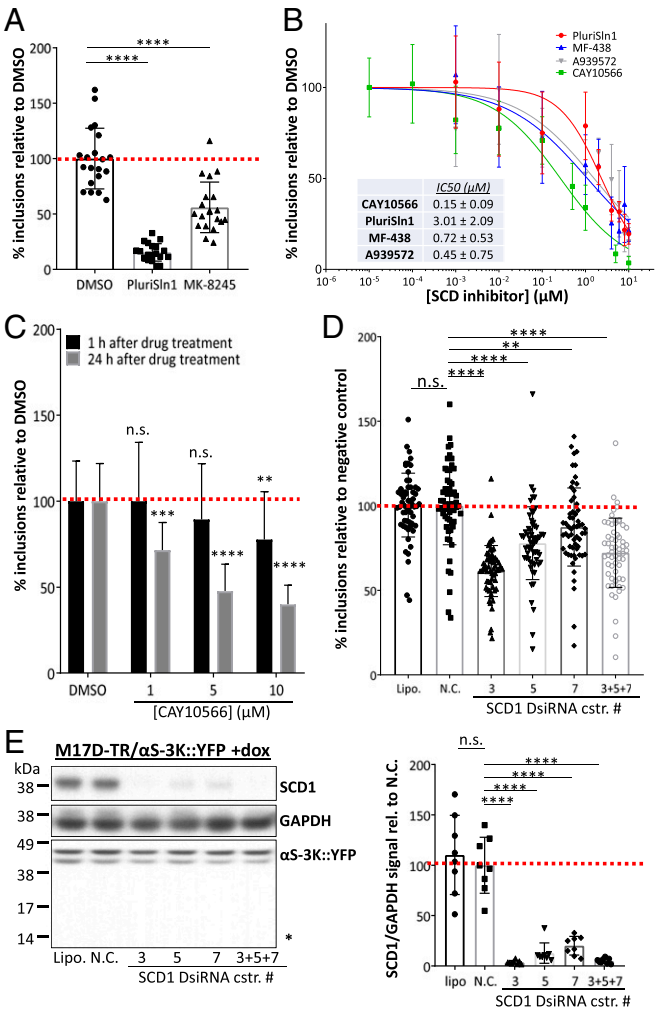

Fig. 5. Pharmacological inhibition and genetic knockdown of SCD clear αS inclusions. (*A*) Retest and confirmation of the 2 SCD inhibitors identified in the screen. M17D-TR/αS-3K::YFP pretreated for 24 h with 10 μM PluriSln1 or MK-8245 and then induced. Inclusions quantified 24 h after induction (normalized to constitutive mCherry and expressed as a percentage of DMSO control; $n = 20$). (*B*) Dose–response and fitted curves of 3 other commercially available SCD inhibitors compared to PluriSln1; for each drug, the concentration that inhibits inclusion formation by 50% (IC_{50}) was calculated (norm. to const. mCherry, percentage of DMSO, $n = 12$ for DMSO and $n = 6$ for drugs). (*C*) Rescue effect of CAY10566: cells induced for 24 h and then treated with 1, 5, or 10 μM CAY10566. Inclusions quantified 1 h after treatment (black bars) or 24 h after treatment (gray bars), normalized to constitutive mCherry, percentage of DMSO vehicle; $n = 12$ (DMSO) or $n = 24$ (compounds). (*D*) M17D-TR/αS-3K::YFP treated for 48 h with either a single DsiRNA targeting SCD1, a mix of these DsiRNAs, a nontargeting control (N.C.), or Lipofectamine alone, then induced for 24 h. Inclusions quantified (norm. to const. mCherry, percentage of DMSO vehicle). (*E*) After imaging, WB for SCD1, GAPDH, and αS (mAb 15G7); asterisk indicates endogenous αS. Quantification of SCD1 knockdown normalized to GAPDH (expressed as percentage relative to N.C.; $n = 8$). Graphs are means ± SD. Criteria for significance relative to controls were $^{*}P < 0.05$, $^{**}P < 0.01$, $^{***}P < 0.001$, and $^{****}P < 0.0001$; n.s., not significant.

across samples (Fig. 6*A*). CAY10566 also decreased pS129 (Fig. 6*B*). An alternative method for assessing αS multimer:monomer dynamics in live cells is the use of a YFP complementation assay (24, 39). Following pretreatment with 10 μM CAY10566 for 24 h, M17D cells were transfected with separate constructs expressing αS 3K fused to a split YFP reporter (24). Higher YFP complementation was observed in CAY10566-treated cells, indicative of increased multimerization (Fig. 6*C*). To confirm relevance to the clinical mutation, M17D cells expressing αS E46K were treated with 10 μM CAY10566 for 48 h. WB revealed increased αS60:14 ratios upon cross-linking, DJ-1 was unchanged (Fig. 6*D*), and pS129 was also decreased (Fig. 6*E*; non–cross-linked samples).

We previously reported that the transient expression of αS 3K causes frank toxicity in M17D cells in various assays (24). We sought to recapitulate this finding in an image-based assay by programming the IncuCyte software to differentiate between live cells (flat) and dead cells (rounded). This approach also revealed a pronounced decrease in viability of αS 3K transfectants vs. WT, while slight differences in E46K vs. wt did not reach significance (Fig. 7 *A* and *B*). When we treated parental M17D cells for 24 h with 10 μM of CAY10566 before transfection, the number of dead 3K::YFP expressing cells was markedly decreased (Fig. 7*B*). Transgene expression was unaffected by SCD inhibition (Fig. 7 *C* and *D*).

FA Treatment Affects Inclusions and αS Homeostasis. Given the role of SCD in converting SFAs to MUFAs, we hypothesized that SCD inhibition mitigates dyshomeostasis by increasing the relative cellular concentration of SFAs. As a proof of concept that SFAs are beneficial and MUFAs are deleterious, M17D cells constitutively expressing αS E46K were "FA-loaded" with SFAs myristic acid (C14:0), palmitic acid (C16:0), or stearic acid (C18:0) or MUFAs palmitoleic acid (C16:1) and oleic acid (OA; C18:1). Following 24 h conditioning, all SFAs (C14:0, C16:0, and C18:0) significantly decreased pSer129 levels, whereas both MUFAs (C16:1 and 18:1) strongly increased pSer129 (Fig. 8*A*). Moreover, at least C14:0 significantly elevated αS60:14 ratios, while both C16:1 and C18:1 significantly decreased αS60:14 ratios (Fig. 8*B*). We obtained similar results in the αS-3K model, where we could also test for inclusions: all of the SFAs tested (C14:0, C15:0, C16:0, and C18:0) decreased 3K::YFP inclusions in a dose-dependent manner, and C18:1 increased them (*SI Appendix*, Fig. S9 *A* and *B*) (interestingly, shorter chain-length SFAs exhibited lower IC_{50} values). pS129 of untagged αS 3K was lowered and αS60:14 ratios were increased by SFAs; MUFAs had the opposite effects (*SI Appendix*, Fig. S9 *C* and *D*).

SCD Inhibitors Affect WT and E46K αS Homeostasis in Human Neurons. Next, induced pluripotent stem cells (iPSCs) were lentivirus-transduced (human wt αS, E46K αS, parental vector) and differentiated into "induced neurons" (iNs) via neurogenin-2 (40). After 14-d differentiation, cultures were treated with 10 μM CAY10566 for 4 d. Following the treatment, immunocytochemistry confirmed the presence of neuronal markers (MAP2, NeuN, β3-tubulin) and αS overexpression (Fig. 9*A* and *SI Appendix*, Fig. S10). As expected (24), E46K iNs had decreased αS60:14 ratios vs. WT and increased pS129 (DMSO controls in Fig. 9 *B* and *C*). Treatment of αS wt or E46K iNs with CAY10566 increased αS60:14, while DJ-1 dimer:monomer ratios were unaffected (Fig. 9*B*). Two other SCD inhibitors, A939572 and MF-438, also increased αS60:14 in E46K iNs (*SI Appendix*, Fig. S11). Moreover, in both αS wt and αS E46K iNs, CAY10566 reduced pS129 signals to similar basal levels (Fig. 9*C*). Finally, it has been demonstrated that αS transiently interacts with vesicle membranes (2, 12). This interaction is abnormally enhanced by E46K, perhaps via increased electrostatic interactions of the positive lysine with negatively charged phospholipid headgroups (16). Indeed, increased αS membrane association has been proposed to be a starting point for abnormal αS aggregation (41). To examine αS membrane interactions, we performed sequential protein extraction of CAY10566- vs. control-treated E46K iNs. Cells exposed to the SCD inhibitor showed lower ratios of membrane-associated (Triton X-100 fraction) vs. cytosolic (PBS fraction) αS (Fig. 9*D*).

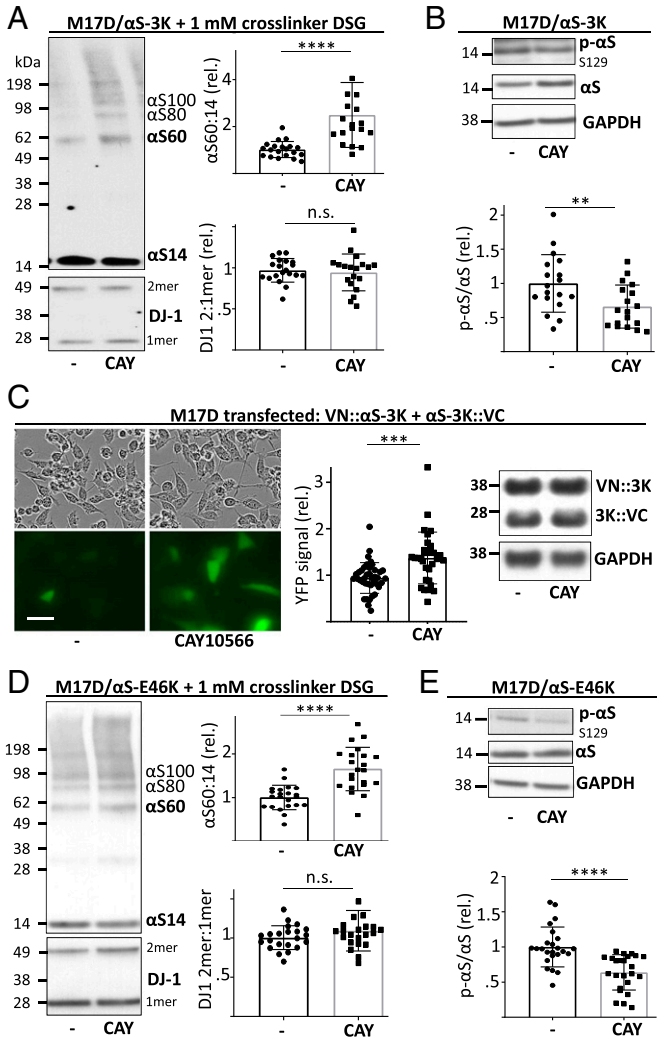

Fig. 6. SCD inhibitor CAY10566 affects αS 3K and E46K biochemical properties in M17D cells. (*A*) M17D/αS-3K cells treated for 48 h with 10 μM CAY10566 or DMSO alone. DSG (1 mM) intact-cell cross-linking and WB for total αS (mAb 15G7) and DJ-1 (control for equal cross-linking and loading). Quantification of αS60:14 and DJ-1 dimer:monomer ratios (normalized to DMSO vehicle; $n = 12$). (*B*) M17D/αS-3K cells treated for 48 h with 10 μM CAY10566 or DMSO alone. WB for αS pS129, total αS (mAb 15G7), and GAPDH (loading control). Quantification of pS129:total αS ratios (normalized to DMSO; $n = 18$). (*C*) Representative bright-field images and YFP signals resulting from split-YFP complementation (VN::αS-3K and 3K-αS::VC). Transfected M17D cells treated for 24 h with 10 μM CAY10566 or DMSO, plus quantification (DMSO set to 1; $n = 39$ for DMSO, $n = 32$ for CAY). Representative WB for αS (mAb 15G7) and GAPDH. (Scale bar, 50 μm.) (*D*) Analogous to *A*, but αS E46K ($n = 22$). (*E*) Analogous to *B*, but αS E46K ($n = 24$). Graphs are means ± SD. Criteria for significance were $^{**}P < 0.01$, $^{***}P < 0.001$, and $^{****}P < 0.0001$; n.s., not significant.

Discussion

The lack of simple, reproducible cellular models of αS dyshomeostasis has made high-throughput screens in human cells challenging: the expression of even high levels of wt or fPD αS does not readily lead to αS aggregation or toxicity in cell culture (24). Indeed, it has been reported that YFP-tagged αS-A53T will only form inclusions in cultured cells after one adds MSA brain homogenates (42). Similarly, recombinant αS preformed fibrils (43, 44) have been used extensively by several laboratories to induce phenotypes related to αS aggregation. Our αS 3K model is different from these approaches in that αS dyshomeostasis occurs robustly and reproducibly in a cell-autonomous fashion. In cultured cells, αS 3K readily produces pronounced features of αS dyshomeostasis such as formation of round, αS+, and membrane/lipid-rich cytoplasmic inclusions; a decrease in the normal αS multimer:monomer ratio; and frank neurotoxicity (17, 24). To establish a stable αS inclusion reporter cell line not confounded by continuous toxicity, we have created here a dox-inducible system of YFP-tagged αS 3K in M17D human neuroblastoma cells.

Characterizing Known and New Modifiers of αS Biology. Multiple observations support the concept that αS 3K cells model excessive αS membrane binding. E46K alone exhibits stronger binding to vesicle membranes than does wt αS (16), and this is further amplified in 3K (E35K+E46K+E61K) (25). Accordingly, αS 3K inclusions that are membrane/lipid-rich (17) (Fig. 1) arise from αS–membrane interactions that are stronger than WT, but mediated by the same principal mechanism, initial formation of membrane-induced amphipathic helices (25). The fast dissolution of 3K inclusions after certain experimental treatments (Figs. 3 and 4 and Movie S2) and dynamics of untreated inclusions (Fig. 4*A* and Movie S1) is not consistent with the presence of amyloid fibers and large amyloid aggregates but rather suggests dynamic assemblies of excess αS monomers, bound to local membranes and lipid droplets. Importantly, such membrane/lipid-rich αS accumulations have been described as a feature of human Lewy cytopathology previously (45–48), and very recently in an elegant study based on correlative light electron microscopy (5). We found that the lipid-related PD drug candidate miglustat as well as published αS-modifying compounds such as isradipine (19), nilotinib (20), fingolimod (21), NOR (22), TFP (23), FK506 (26), squalamine (27), trodusquemine (28), and PcTS (29) each reduced αS 3K inclusion burden (Fig. 2 and *SI Appendix*, Fig. S4), whereas there was no decrease with an unrelated drug [tafamidis (33)] or certain compounds with unclear therapeutic relevance to PD [nicotine (30), caffeine (30), statins (33, 34)]. αS levels per se were largely unaffected by the inclusion-clearing compounds (*SI Appendix*, Fig. S6), suggesting a mode of action via preventing excess αS membrane binding. To further probe the mechanisms of such compounds, our model enables kinetic analyses. NOR has been proposed to directly bind to soluble αS, thereby inhibiting its pathological aggregation (22). Consistent with that, NOR dissolved preexisting αS 3K inclusions within 1 h. The equally fast action of TFP suggests a similar mechanism (Figs. 3 and 4 and Movies S1 and S2). Nilotinib (20), fingolimod (21), FK506 (26), and PcTS (29) also markedly reduced preexisting αS inclusions within 1 h (Fig. 3). Such rapid effects could mean (1) a direct influence of the compound on αS homeostasis by binding to certain species within the αS folding landscape or (2) rapid compound effects on the cellular milieu such as altered ion levels. Slow action would be more consistent with indirect effects on αS by gradually altering metabolic processes. SCD inhibitors, an emerging class of modifiers of αS biology (as detailed later), apparently act on αS homeostasis by altering membrane FA composition (Fig. 10). In accord with this hypothesis, SCD inhibitors strongly reduced inclusions by 24 h but barely after 1 h of treatment (Fig. 5*C*). Complete lack of action (here, nicotine and caffeine) is inconsistent with effects on αS–membrane interaction, but any such drug may still affect PD-relevant biology by different mechanisms: e.g., interfering with non–membrane-mediated αS aggregation, non–cell-autonomous mechanisms of αS dyshomeostasis (neuron–glia interplay; spreading), or αS-independent mechanisms. Thus, our relatively fast and simple assay offers a tool to help characterize compounds of potential relevance for PD, especially in comparative studies that also include in vivo models and other cellular readouts such as preformed fibril (45, 46) models that may cover additional aspects of PD-relevant biology.

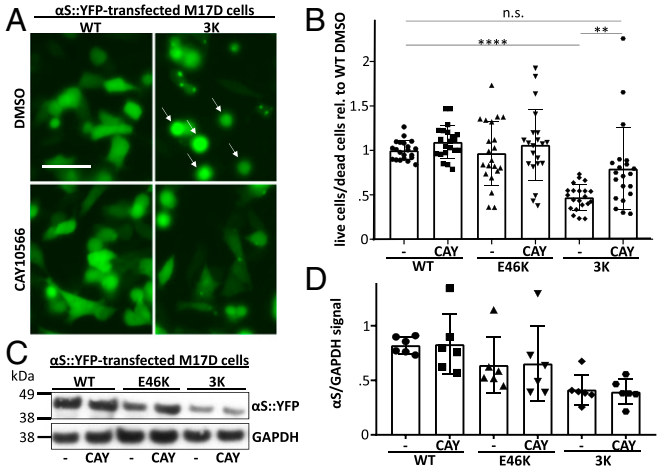

Fig. 7. SCD inhibitor CAY10566 rescues αS toxicity in M17D cells. (*A*) M17D cells treated for 24 h with DMSO or CAY10566, then transfected with YFP-tagged αS WT, E46K, and 3K. Representative YFP images (WT, 3K). (Scale bar, 50 μm.) (*B*) Quantification of live/dead YFP^+ cells (WT DMSO set to 1). (*C*) At 48 h after transfection: WB for total αS (mAb 15G7) and GAPDH. (*D*) Quantification of αS/GAPDH ratios. Graphs are means ± SD. Criteria for significance were $^{**}P < 0.01$ and $^{****}P < 0.0001$; n.s., not significant.

Discovering New Modifiers of αS Biology. After establishing our 3K assay and using it to characterize several reported αS-relevant compounds, we blindly screened a bioactive library in a 384-well plate format. Among interesting hits, 2 compounds (PluriSln1 and MK-8245) emerged that are known inhibitors of SCD, the rate-limiting enzyme for conversion of SFAs into MUFAs. After validating the benefits of PluriSln1 and MK-845, we examined 3 additional SCD inhibitors: MF438, A939572, and CAY10566. All 5 inhibitors dose-dependently decreased αS inclusions; CAY10566 had the lowest IC_{50}, 150 nM (Fig. 5*B*). The inclusion decrease was paralleled by salutary biochemical effects: increased αS multimer:monomer ratios (αS60:14), less S129 phosphorylation (3K, E46K, wt αS) (Figs. 6 and 9), and more physiological αS cytosol:membrane partitioning (E46K) (Fig. 9*D*). Importantly, the promotion of αS 3K multimerization was confirmed by 2 very different cellular assays: intact-cell cross-linking (Fig. 6*A*) and YFP complementation (Fig. 6*C*). Upon SCD inhibition in iPSC-derived neurons, we observed increased αS60:14 and decreased pS129 not only with E46K but also with wt αS (Fig. 9 *B* and *C*). The latter result underlines that inhibiting SCD is not an E46K-specific strategy but could also benefit excessive levels of wt αS, e.g., duplication or triplication of the SNCA gene. Several findings support the robustness and specificity of the pharmacological treatments. First, SCD inhibitors of different structures conferred similar effects. Second, we observed negative effects of MUFAs added exogenously to cells (inclusions↑, aS60:14↓, pS129↑) and conversely positive effects of SFAs (inclusions↓, pS129↓; αS60:14↑ vs. control became significant only for C14:0 at $n = 9$, presumably due to the greater complexity of this FA-conditioning assay) (Fig. 8). These effects were paralleled by the inclusion-promoting effects of 18:1 and the inclusion-preventing effects of SFAs (*SI Appendix*, Fig. S9). Third, RNAi knockdown of SCD1 reduced αS3K inclusions. The relative inefficiency of the dsiRNAs (15 to 40% depending on construct) vs. the pan-SCD inhibitors appears due to the observed residual SCD1 (the most efficient dsiRNA reduced inclusions by 40%) and/or the unaffected activity of the CNS-specific SCD5 isoform in our neural cells. The lack of SCD5 antibodies precluded confirmation of the later explanation. These findings, together with the evidence that SCD inhibitors beneficially redistribute αS from membranes to cytosol (Fig. 9*D*), are all consistent with a hypothetical unifying model of αS homeostasis (Fig. 10). To wit, SCD inhibition increases the proportion of SFAs in the membrane, while the proportion of MUFAs decreases. The higher levels of SFAs in the membrane lipids decrease membrane fluidity and thus αS–membrane interaction/binding (39). Excess αS monomers at membranes may be cytotoxic, e.g., by interfering with vesicle trafficking (17, 49, 50) or promoting αS aggregation via its primary nucleation (43). The increase in physiologically soluble αS upon SCD inhibition is associated with increased tetramer/multimer formation, an event known to prevent αS aggregation/toxicity (8, 51).

Relevance of Our Assay as a Platform and SCD as a Therapeutic Target. The relevance of our αS 3K and 1K models for PD, DLB, and other synucleinopathies in helping identify mechanisms and targets is supported to date by several observations: 1) αS 3K is a biochemical "amplification" of the fPD-linked E46K; 2) αS 2K (E35K+E46K) and 3K (E35K+E46K+E61K) "dose-dependently"

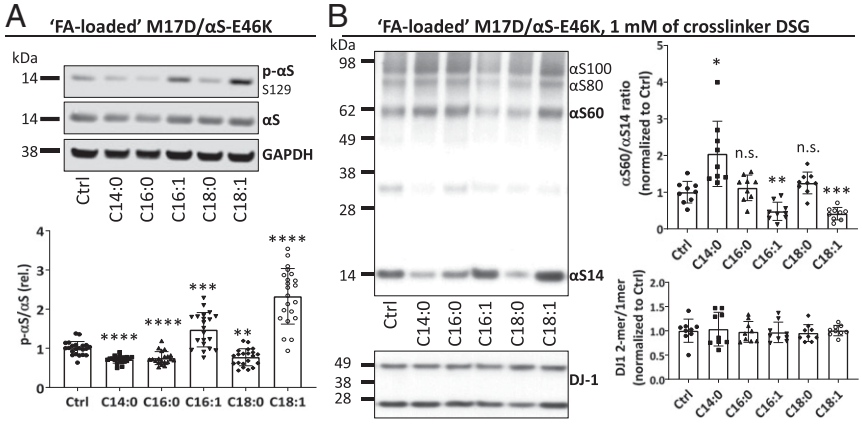

Fig. 8. FA loading affects biochemical properties of αS E46K in M17D cells. (*A*) M17D/αS-E46K cells treated for 24 h with different SFAs (C14:0 myristic acid, C16:0 palmitic acid, or C18:0 stearic acid) or MUFAs (C16:1 palmitoleic acid or C18:1 oleic acid) in FBS-free media. WB and quantification of αS-pS129:total αS ratios (normalized to 1 for the control; $n = 20$ for C14:0 and C16:0, $n = 21$ for C16:1 and C18:0, and $n = 22$ for control and C18:1). (*B*) Analogous to *A*, but 1 mM DSG intact-cell cross-linking. WB for total αS (mAb 15G7) and DJ-1 (control for cross-linking and loading). Quantification of αS60:14 and DJ-1 dimer:monomer ratios after cross-linking (normalized to control; $n = 9$). Graphs are means ± SD. Criteria for significance relative to control were $^{*}P < 0.05$, $^{**}P < 0.01$, $^{***}P < 0.001$, and $^{****}P < 0.0001$; n.s., not significant.

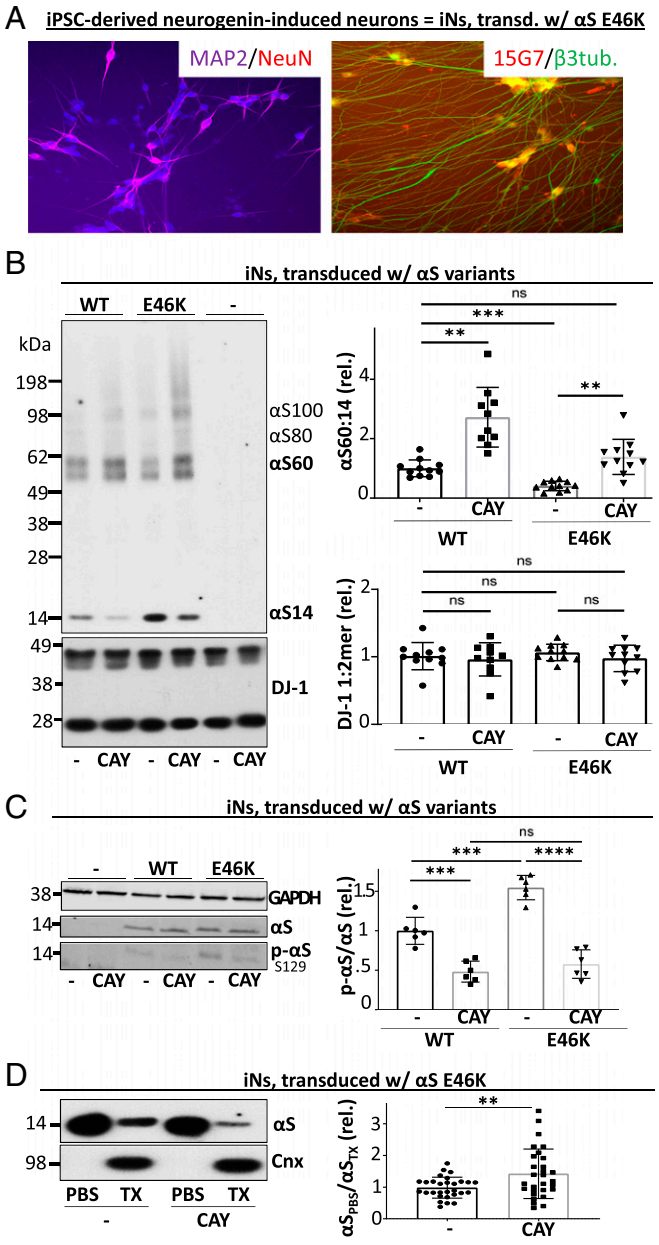

Fig. 9. SCD inhibition restores normal αS homeostasis in human neurons. hiPSCs (line BR2132) expressing parental vector (PV), αS WT, or αS E46K differentiated into iNs for 14 d, then treated for 4 d with 10 μM CAY10566 or DMSO control (fresh media/drug after 2 d). (*A*) Immunofluoresence (IF) of iNs expressing E46K αS at d 18: total αS (mAb 15G7), MAP2, NeuN, and β3-tubulin. (Magnification 40×; scale bar, 50 μm.) (*B*) αS wt and E46K expressing iNs: 1 mM DSG intact-cell cross-linking at day 18. WB for αS (mAb 15G7) and DJ-1. Quantification of αS60:14 and DJ-1 dimer:monomer ratios: CAY10566 treatment or DMSO vehicle control (normalized to DMSO-treated αS-WT; $n = 11$ except for wt CAY10566, $n = 10$). (*C*) WBs for αS-pS129, total αS, and GAPDH as a loading control. Quantification of αS-pS129:total αS ratios (normalized to DMSO vehicle; $n = 6$). (*D*) Sequential extraction of iNs expressing E46K αS treated for 4 d with 10 μM CAY10566 or DMSO control (fresh media/drug after 2 d). WB for αS and calnexin (membrane marker). Quantification of αS cytosol:membrane ratios. Graphs are means ± SD. Criteria for significance were $^{**}P < 0.01$, $^{***}P < 0.001$, and $^{****}P < 0.0001$; ns, not significant.

accentuate the subtle cellular phenotypes of 1K (fPD E46K) like less solubility, more inclusion formation, and neurotoxicity (24); 3) αS 3K expression in cells causes lipid/membrane vesicle-rich αS accumulation similar to that described in Lewy neuropathology (5, 47–50); 4) αS 3K mice develop (at a rather young age) a striking DOPA-responsive motor syndrome closely resembling PD (18); and 5) compounds reported as modulators of wt or fPD αS alterations and thus potential PD drugs can markedly reduce αS 3K inclusions, whereas control compounds do not (Figs. 2 and 3). Despite all of these concordant findings, we emphasize here that the 3K cellular model 1) does not necessarily model all aspects of αS dyshomeostasis (discussed earlier); 2) is a discovery platform, and any findings require validation in fPD αS single-mutant and excess wt αS models, as shown here for SCD. SCD inhibition also reduced αS cytotoxicity in our study; we quantified the pronounced cytotoxicity of αS 3K in cultured cells (24) by automated microscopy (Fig. 7). Support for the prevention of wt αS-related toxicity by SCD inhibition comes from 2 very recent studies. Fanning et al. (52) explored SCD inhibition after observing OA (18:1) increases upon lipid profiling of αS-expressing yeast. The study showed that SCD inhibition prevents αS-wt toxicity in yeast and in worm and rodent neurons. Independently, Vincent et al. (53) identified SCD as a PD-relevant target in an unbiased viability screen in yeast expressing αS. These 2 reports, coupled with the present study, lead us to propose that a MUFA (OA) that is up-regulated by αS (52) can in turn render αS more toxic and prone to inclusions, reminiscent of a "bidirectional pathogenic loop" proposed for αS and GCAse (6). Now that SCD has emerged as an αS-relevant target in 3 independent studies, it will be important to establish its in vivo relevance in a mouse PD model such as the new αS 3K mouse (18).

Materials and Methods

cDNA Constructs and Viruses. Plasmids pcDNA4/αS (10), pcDNA4/αS-E46K (24), pcDNA4/αS-3K (24), pcDNA4/αS-3K::YFP, pcDNA4/VN::αS-3K (24), and pcDN4/VC::αS-3K (24), as well as pLVX-EF1a/αS-IRES-mCherry (17) lentiviral plasmids for wt and 3K have been described (the E46K lentiviral construct was generated in an analogous fashion) (24).

Cell Culture, Stable Cell Lines, and Induced Neurons. Human neuroblastoma cells [BE (2)-M17 = M17D; ATCC number CRL-2267] were cultured in Dulbecco's modified Eagle's medium (DMEM) supplemented with 10% FBS, 50 U/mL penicillin, 50 μg/mL streptomycin, and 2 mM L-glutamine. αS-3K::YFP expression in M17D-TR/αS-3K::YFP/RFP (17) was induced with 1 μg/mL final concentration of doxycycline HCL (dox). Stable cell pools M17D/αS-E46K and M17D/αS-3K were generated by transducing M17D cells with wt or E46K pLVX-EF1a/αS-IRES-mCherry (17) lentiviral particles. iPSC-derived neurogenin-induced human neurons (iNs) were prepared from the BR2132 iPSC line from a healthy individual (54). Neuronal differentiation and culture were as described previously (55) with slight modification: TetO-GFP virus was omitted and pre differentiation pLVX-EF1a/αS-IRES-mCherry (17) lentiviral particles for WT, E46K, and 3K were added.

Transfection of αS::YFP Constructs and Live-Cell Microscopy. M17D cells were transfected with pCAX/dsRed and YFP-tagged αS variants using Lipofectamine 2000 following the manufacturer's directions (24). Cells were analyzed

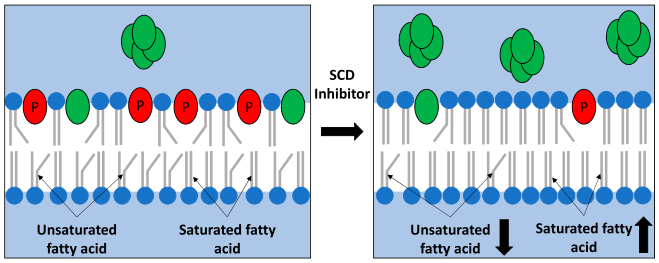

Fig. 10. Hypothesis on how SCD inhibition rescues αS dyshomeostasis. Treating cells with SCD inhibitors decreases monounsaturated FAs (MUFAs) and increases saturated FAs (SFAs) in cellular membranes. This reduces the binding of monomeric αS to the membranes and αS-pS129 levels, a marker for αS dyshomeostasis. The number of soluble, aggregation-resistant αS multimers increases.

by fluorescent microscopy 24 h after transfection. Bright-field and fluorescence microscopy of live cells in culture dishes was as published (24) (AxioVert 200 microscope; AxioCam MRm camera; AxioVision Release 4.8.2; Zeiss). Analyses were performed in a blinded fashion by assigning random numbers to culture dishes before representative images for each culture were taken. Image collections were blinded before cells (+/– inclusions) and were counted by another investigator.

Imaging and High-Throughput Screen. Inclusion formation was recorded in 2-h intervals in M17D-TR/αS-3K::YFP//RFP cells (96- or 384-well plates) on an IncuCyte Zoom machine (Essen Bioscience). Constitutive mCherry signal, total YFP integrated intensity, and YFP inclusion integrated intensity were quantified using the IncuCyte software and analysis jobs described in *SI Appendix*, Table S2 (columns A–C). Toxicity was assessed via the ratio of mCherry 24 h/1 h after induction. For the inclusions, the graphs represent the integrated intensity of YFP inclusions over the mCherry signal to normalize to cell number. Each point represents 1 individual well. The 1,902 compounds in the Selleck bioactive library were screened at ICCB Longwood (Harvard Medical School) using TFP as a positive control (10 μM, 0.1% DMSO). A total of 10,000 cells per well of a 384-well plate were plated on day 1; on day 2, drugs (10 μM, or 0.1% vol/vol) were pin-transferred (Seiko D-TRAN XM3106-31 PN 4-axis cartesian robot controlled by an SRC-310A controller coupled with an Epson C3-A601S 6-axis robot controlled by an RC-620 controller). Immediately after treatment, cells were induced and incubated for 24 h. On day 3, cells were fixed with 4% paraformaldehyde and stained with Hoechst dye (Invitrogen; H3570). Plates were scanned in a GE InCell2200. Images were analyzed and inclusions and nuclei were quantified using an in-house script running on CellProfiler; effects on inclusions (green channel) and nuclei (blue channel) were calculated in a custom script in R. Both are available in a GitHub repository (https://github.com/SubstantiaNegri/alphaSynScreen).

Electron Microscopy. Cells were fixed in 2.5% glutaraldehyde, 1.25% paraformaldehyde, 0.03% picric acid in 0.1 M sodium cacodylate buffer (pH 7.4) and analyzed by EM as published (17).

Drug Treatments. In the prevention paradigm, cells were plated on day 1, treated with drugs on day 2, and induced on day 3. In the rescue paradigm, cells were plated on day 1, induced on day 2, and treated with drugs on day 3 after ensuring similar inclusion levels. TFP and NOR short-term treatments were done as specified in Fig. 4 and *SI Appendix*, Fig. S12.

SCD1 Knockdown. SCD1 DsiRNAs (IDT) were no. 3 (hs.Ri.SCD.13.3), no. 5 (hs.Ri.SCD.13.5), and no. 7 (hs.Ri.SCD.13.7), plus scramble DsiRNA (NC-5) as a negative control. For transfection, Lipofectamine RNAiMAX (Thermo Fisher; 1378030) was used. At 48 h after transfection, cells were induced, and inclusion formation was followed in the IncuCyte for 24 h.

Free FA Loading. Free FAs used were myristic acid, pentadecanoic acid, palmitic acid, palmitoleic acid, stearic acid, and OA (structures and references in *SI Appendix*, Fig. S12). αS-3K::YFP cells were plated on day 1 without FBS (starving condition) and treated on day 2 with various concentrations of bovine serum albumin (BSA)/FA complexes (38). To prepare BSA/FA complexes, BSA was mixed with FAs at a ratio of 1:5 before 30 min of incubation in a binding buffer (10 mM Tris HCl [pH 8.0], 150 mM NaCl). Various concentrations of BSA/FA complex were added to cells. For the inclusion assay, cells were induced 6 h after applying the BSA/FA mix and inclusion formation was followed via IncuCyte and analyzed 24 h after induction. Cross-linking and pS129 assays were performed after 24 h of incubation with the BSA/FA complex without FBS.

Cross-Linking. DSG (1 mM) cross-linking was performed as previously described (56). For iNs, in-well cross-linking was performed in 24-well plates: cells were washed with 400 μL of HBSS. Then, 400 μL 0.5 mM DSG in HBSS were added to each well, and incubation and quenching were as published (56). DSG solutions were then aspirated, and attached cells were lysed (as detailed later).

Complementation Assay. M17D cells were plated in 96-well plates at 10,000 cells per well on day 1 and treated with 0.1% DMSO or 10 μM CAY10566 on day 2. At 24 h after treatment, cells were transiently transfected using Lipofectamine 3000 with 75 ng αS-3K::VC and 25 ng VN::αS-3K (24) per well. Then, YFP was monitored in the IncuCyte for 24 h via the total YFP integrated intensity algorithm (*SI Appendix*, Table S2, column B).

Protein Extraction. To generate total protein lysates (cytosolic and membrane proteins), cells were lysed in 1% Triton X-100 detergent (TX-100; Sigma, 9002–93-1) in PBS containing protease inhibitors (PIs) and sonicated for 15 s, followed by centrifugation for 30 min at 21,000 × *g*. Protein concentrations were determined by BCA assay. LDS sample buffer was added followed by boiling. For iNs, cross-linked cells in the dish were resuspended in 75 μL of PBS, and 25 μL of 4× LDS was added before samples were sonicated for 15 s and boiled. For pS129 detection, cells were lysed in TBST/PI/phosphatase inhibitor/1% TX-100.

Sequential Extraction in iNs. Cells were resuspended in their media, transferred to 1.5-mL tubes, and centrifuged at 1,500 × *g* for 5 min. Pellets were resuspended in 100 μL of ice-cold water and incubated on a rotating wheel at 4 °C for 5 min. A total of 11 μL of 10× PBS was added, followed by ultracentrifugation at 100,000 × *g* for 30 min at 4 °C. Supernatants were collected (cytosolic fraction), and pellets were resuspended in 111 μL of 1× PBS 1% TX-100 and sonicated for 15 s. After 10 min on ice, tubes were ultracentrifuged again and supernatants were collected (membrane fraction). To improve WB detection, all fractions were cross-linked with 2 mM DSP (Thermo Fisher; 20593) for 30 min at 37 °C (9), followed by reductive cleavage (boiling in sample buffer + 5% β-mercaptoethanol f.c.).

Immunoblotting. Protein samples were run on NuPAGE 4 to 12% Bis-Tris gels (Invitrogen) at 100 V and transferred in the iBlot 2 system (Invitrogen) to nitrocellulose membranes (iBlot 2 NC regular stacks; IB23001; pS129 samples) or PVDF membranes (iBlot 2 PVDF regular stacks; IB24001; all other samples). Membranes were fixed for 10 min in 0.4% PFA (in PBS; TBS for pS129 samples). PVDF membranes were blocked in blocking buffer (0.2% Tropix I-Block in PBST) for 1 h and incubated in primary antibody in blocking buffer for 1 h at room temperature or o/n at 4 °C. Membranes were washed 5 × 5 min in PBST, and secondary antibodies in blocking buffer were added for 1 h at RT. Membranes were washed 5 × 5 min in PBST, and ProSignal Dura ECL (Prometheus Protein Biology Products, ref. 20–301B) was added for 2 min before exposing. Nitrocellulose membranes were blocked in Odyssey Blocking Buffer, TBS (Li-Cor, ref. 927–50000) for 1 h. Membranes were incubated with GAPDH, 15G7 (total αS), and pS129 antibodies in Odyssey Blocking Buffer, TBS, 0.2% Tween 20, and washed 5 × 5 min in TBST. Secondary antibodies were prepared in the same buffer and added for 1 h at RT, protected from light. Membranes were washed 5 × 5 min in TBST and scanned (Odyssey CLx, Li-Cor).

Immunocytochemistry. At day 18 of differentiation, iNs were fixed in 4% PFA in PBS for 10 min and washed 3 × 5 min in PBS. Cells were then permeabilized in PBS/1% TX-100 for 10 min and washed 3 × 5 min with PBS. First antibodies were prepared in TBS/10% goat serum and incubated for 1 h at RT. Cells were washed 3 × 5 min in PBS and incubated for 1 h with secondary antibodies in TBS/10% goat serum. Cells were washed 3 × 5 min in PBS and imaged on InCell2200.

Cytotoxicity Assay. A total of 10,000 M17D cells per well (96-well plate) were plated on day 1 and treated with 0.1% DMSO or 10 μM CAY10566 on d 2. At 24 h after treatment, each well was transfected with 55 ng of DNA, 0.1 μL Lipofectamine 3000, and 0.1 μL P3000 reagent. DNA constructs were pcDNA4 parental vector (PV), αS-WT::YFP, αS-K::YFP, αS-3K::YFP, or YFP. IncuCyte images (24 h post transfection) were analyzed using processing definitions described in *SI Appendix*, Table S2 (columns D, E) to quantify green rounded dead cells and green flat live cells. Dead/live cell ratios were calculated.

Drugs. All drugs are listed in *SI Appendix*, Fig. S12 with their structure and reference.

Antibodies. All antibody names, references, and dilutions are listed in *SI Appendix*, Table S3.

Statistical Analyses. We performed 1-way ANOVA including Tukey's (Figs. 3 *A* and *B*, 5 *C* and *E*, 7 *B*, and 9*C*) or Dunnett's (Figs. 1*A*, 2*E*, and 5 *A* and *D*) multiple comparisons test, Brown–Forsythe, and Welsh ANOVA including Dunnett's T3 multiple-comparison test (Figs. 8 *A* and *B* and 9*B*), and unpaired, 2-tailed *t* tests (Figs. 2 *A–C*, 6 *A–E*, and 9*D*) using GraphPad Prism version 8 following the program's guidelines. Normal distribution and equal variance were observed for all values except for Figs. 8 *A* and *B* and 9*B* (as detailed earlier). Graphs represent means ± SD. Criteria for significance, routinely determined relative to untreated WT, were: $*P < 0.05$, $**P < 0.01$,

***$P < 0.001$, ****$P < 0.0001$. Sufficient experiments and replicates were analyzed to achieve statistical significance, and these judgements were based on earlier, similar work. Outliers automatically detected by GraphPad Prism were excluded using the "identify outliers" tool with the ROUT method and Q = 1%.

ACKNOWLEDGMENTS. We thank T. Bartels, V. Khurana, S. Nuber, J. di Bernardo, and J. Boyd for their advice on this project; V. Lagomarsino and L. Sanz and for advice on imaging; M. Ericsson for EM images; J. Smith and S. Rudnicki at the ICCB for their help with the compound screen; C. Muratore (iPSC NeuroHub at the Ann Romney Center for Neurologic Diseases) and M. Liao for advice on iPSC-derived neuron cultures; N. Exner and C. Haass (Munich) for mAb 15G7; and Nicole Boucher for her administrative support. This work was supported by NIH Grants NS099328 (to U.D.), NS083845 (to D.S.), and NS065743 (to G.P.H.H.).

1. H. Fujiwara *et al*., alpha-Synuclein is phosphorylated in synucleinopathy lesions. *Nat. Cell Biol.* **4**, 160–164 (2002).
2. L. Maroteaux, R. H. Scheller, The rat brain synucleins; family of proteins transiently associated with neuronal membrane. *Brain Res. Mol. Brain Res.* **11**, 335–343 (1991).
3. J. J. Zarranz *et al*., The new mutation, E46K, of alpha-synuclein causes Parkinson and Lewy body dementia. *Ann. Neurol.* **55**, 164–173 (2004).
4. A. B. Singleton *et al*., alpha-Synuclein locus triplication causes Parkinson's disease. *Science* **302**, 841 (2003).
5. S. H. Shahmoradian *et al*., Lewy pathology in Parkinson's disease consists of crowded organelles and lipid membranes. *Nat. Neurosci.* **22**, 1099–1109 (2019).
6. J. R. Mazzulli *et al*., Gaucher disease glucocerebrosidase and α-synuclein form a bidirectional pathogenic loop in synucleinopathies. *Cell* **146**, 37–52 (2011).
7. S. Kim *et al*., GBA1 deficiency negatively affects physiological α-synuclein tetramers and related multimers. *Proc. Natl. Acad. Sci. U.S.A.* **115**, 798–803 (2018).
8. T. Bartels, J. G. Choi, D. J. Selkoe, α-Synuclein occurs physiologically as a helically folded tetramer that resists aggregation. *Nature* **477**, 107–110 (2011).
9. A. J. Newman, D. Selkoe, U. Dettmer, A new method for quantitative immunoblotting of endogenous α-synuclein. *PLoS One* **8**, e81314 (2013).
10. U. Dettmer, A. J. Newman, E. S. Luth, T. Bartels, D. Selkoe, In vivo cross-linking reveals principally oligomeric forms of α-synuclein and β-synuclein in neurons and non-neural cells. *J. Biol. Chem.* **288**, 6371–6385 (2013).
11. M. Rovere, J. B. Sanderson, L. Fonseca-Ornelas, D. S. Patel, T. Bartels, Refolding of helical soluble α-synuclein through transient interaction with lipid interfaces. *FEBS Lett.* **592**, 1464–1472 (2018).
12. W. S. Davidson, A. Jonas, D. F. Clayton, J. M. George, Stabilization of alpha-synuclein secondary structure upon binding to synthetic membranes. *J. Biol. Chem.* **273**, 9443–9449 (1998).
13. S. Chandra, X. Chen, J. Rizo, R. Jahn, T. C. Südhof, A broken alpha -helix in folded alpha -Synuclein. *J. Biol. Chem.* **278**, 15313–15318 (2003).
14. C. C. Jao, B. G. Hegde, J. Chen, I. S. Haworth, R. Langen, Structure of membrane-bound alpha-synuclein from site-directed spin labeling and computational refinement. *Proc. Natl. Acad. Sci. U.S.A.* **105**, 19666–19671 (2008).
15. U. Dettmer, Rationally designed variants of α-Synuclein illuminate its *in vivo* structural properties in health and disease. *Front. Neurosci.* **12**, 623 (2018).
16. J. D. Perlmutter, A. R. Braun, J. N. Sachs, Curvature dynamics of alpha-synuclein familial Parkinson disease mutants: Molecular simulations of the micelle- and bilayer-bound forms. *J. Biol. Chem.* **284**, 7177–7189 (2009).
17. U. Dettmer *et al*., Loss of native α-synuclein multimerization by strategically mutating its amphipathic helix causes abnormal vesicle interactions in neuronal cells. *Hum. Mol. Genet.* **26**, 3466–3481 (2017).
18. S. Nuber *et al*., Abrogating native α-Synuclein tetramers in mice causes a L-DOPA-responsive motor syndrome closely resembling Parkinson's disease. *Neuron* **100**, 75–90.e5 (2018).
19. C. S. Chan *et al*., 'Rejuvenation' protects neurons in mouse models of Parkinson's disease. *Nature* **447**, 1081–1086 (2007).
20. M. L. Hebron, I. Lonskaya, C. E.-H. Moussa, Nilotinib reverses loss of dopamine neurons and improves motor behavior via autophagic degradation of α-synuclein in Parkinson's disease models. *Hum. Mol. Genet.* **22**, 3315–3328 (2013).
21. G. Vidal-Martínez *et al*., FTY720/Fingolimod reduces synucleinopathy and improves gut motility in A53T mice: Contributions OF pro-brain-derived neurotrophic factor (PRO-BDNF) and mature BDNF. *J. Biol. Chem.* **291**, 20811–20821 (2016).
22. T. J. Collier *et al*., Nortriptyline inhibits aggregation and neurotoxicity of alpha-synuclein by enhancing reconfiguration of the monomeric form. *Neurobiol. Dis.* **106**, 191–204 (2017).
23. M. Höllerhage *et al*., Trifluoperazine rescues human dopaminergic cells from wild-type α-synuclein-induced toxicity. *Neurobiol. Aging* **35**, 1700–1711 (2014).
24. U. Dettmer *et al*., Parkinson-causing α-synuclein missense mutations shift native tetramers to monomers as a mechanism for disease initiation. *Nat. Commun.* **6**, 7314 (2015).
25. M. Rovere *et al*., E46K-like α-synuclein mutants increase lipid interactions and disrupt membrane selectivity. *J. Biol. Chem.* **294**, 9799–9812 (2019).
26. G. Caraveo *et al*., Calcineurin determines toxic versus beneficial responses to α-synuclein. *Proc. Natl. Acad. Sci. U.S.A.* **111**, E3544–E3552 (2014).
27. M. Perni *et al*., A natural product inhibits the initiation of α-synuclein aggregation and suppresses its toxicity. *Proc. Natl. Acad. Sci. U.S.A.* **114**, E1009–E1017 (2017).
28. M. Perni *et al*., Multistep inhibition of α-Synuclein aggregation and toxicity in vitro and in vivo by trodusquemine. *ACS Chem. Biol.* **13**, 2308–2319 (2018).
29. L. Fonseca-Ornelas *et al*., Small molecule-mediated stabilization of vesicle-associated helical α-synuclein inhibits pathogenic misfolding and aggregation. *Nat. Commun.* **5**, 5857 (2014).
30. K. Wirdefeldt, H.-O. Adami, P. Cole, D. Trichopoulos, J. Mandel, Epidemiology and etiology of Parkinson's disease: A review of the evidence. *Eur. J. Epidemiol.* **26** (suppl. 1), S1–S58 (2011).
31. Y.-C. Lee *et al*., Discontinuation of statin therapy associates with Parkinson disease: A population-based study. *Neurology* **81**, 410–416 (2013).
32. G. Liu *et al*., Statins may facilitate Parkinson's disease: Insight gained from a large, national claims database. *Mov. Disord.* **32**, 913–917 (2017).
33. S. M. Johnson, S. Connelly, C. Fearns, E. T. Powers, J. W. Kelly, The transthyretin amyloidoses: From delineating the molecular mechanism of aggregation linked to pathology to a regulatory-agency-approved drug. *J. Mol. Biol.* **421**, 185–203 (2012).
34. L. Kamentsky *et al*., Improved structure, function and compatibility for CellProfiler: Modular high-throughput image analysis software. *Bioinformatics* **27**, 1179–1180 (2011).
35. R Development Core Team, *A Language and Environment for Statistical Computing* (R Foundation Statistical Computing, 2017).
36. R. Sharon *et al*., The formation of highly soluble oligomers of alpha-synuclein is regulated by fatty acids and enhanced in Parkinson's disease. *Neuron* **37**, 583–595 (2003).
37. B. Nuscher *et al*., Alpha-synuclein has a high affinity for packing defects in a bilayer membrane: A thermodynamics study. *J. Biol. Chem.* **279**, 21966–21975 (2004).
38. E. Rhoades, T. F. Ramlall, W. W. Webb, D. Eliezer, Quantification of alpha-synuclein binding to lipid vesicles using fluorescence correlation spectroscopy. *Biophys. J.* **90**, 4692–4700 (2006).
39. U. Dettmer, A. J. Newman, V. E. von Saucken, T. Bartels, D. Selkoe, KTKEGV repeat motifs are key mediators of normal α-synuclein tetramerization: Their mutation causes excess monomers and neurotoxicity. *Proc. Natl. Acad. Sci. U.S.A.* **112**, 9596–9601 (2015).
40. Y. Zhang *et al*., Rapid single-step induction of functional neurons from human pluripotent stem cells. *Neuron* **78**, 785–798 (2013).
41. C. Galvagnion *et al*., Lipid vesicles trigger α-synuclein aggregation by stimulating primary nucleation. *Nat. Chem. Biol.* **11**, 229–234 (2015).
42. S. B. Prusiner *et al*., Evidence for α-synuclein prions causing multiple system atrophy in humans with parkinsonism. *Proc. Natl. Acad. Sci. U.S.A.* **112**, E5308–E5317 (2015).
43. L. A. Volpicelli-Daley *et al*., Exogenous α-synuclein fibrils induce Lewy body pathology leading to synaptic dysfunction and neuron death. *Neuron* **72**, 57–71 (2011).
44. K. C. Luk *et al*., Pathological α-synuclein transmission initiates Parkinson-like neurodegeneration in nontransgenic mice. *Science* **338**, 949–953 (2012).
45. S. Roy, L. Wolman, Ultrastructural observations in parkinsonism. *J. Pathol.* **99**, 39–44 (1969).
46. L. S. Forno, R. L. Norville, Ultrastructure of Lewy bodies in the stellate ganglion. *Acta Neuropathol.* **34**, 183–197 (1976).
47. K. Hayashida, S. Oyanagi, Y. Mizutani, M. Yokochi, An early cytoplasmic change before Lewy body maturation: An ultrastructural study of the substantia nigra from an autopsy case of juvenile parkinsonism. *Acta Neuropathol.* **85**, 445–448 (1993).
48. M. Nishimura *et al*., Synaptophysin and chromogranin A immunoreactivities of Lewy bodies in Parkinson's disease brains. *Brain Res.* **634**, 339–344 (1994).
49. A. A. Cooper *et al*., Alpha-synuclein blocks ER-Golgi traffic and Rab1 rescues neuron loss in Parkinson's models. *Science* **313**, 324–328 (2006).
50. J. H. Soper *et al*., Alpha-synuclein-induced aggregation of cytoplasmic vesicles in Saccharomyces cerevisiae. *Mol. Biol. Cell* **19**, 1093–1103 (2008).
51. J. Burré, M. Sharma, T. C. Südhof, Definition of a molecular pathway mediating α-synuclein neurotoxicity. *J. Neurosci.* **35**, 5221–5232 (2015).
52. S. Fanning *et al*., Lipidomic analysis of α-Synuclein neurotoxicity identifies stearoyl CoA desaturase as a target for Parkinson treatment. *Mol. Cell* **73**, 1001–1014.e8 (2018).
53. B. M. Vincent *et al*., Inhibiting stearoyl-CoA desaturase ameliorates α-Synuclein cytotoxicity. *Cell Rep.* **25**, 2742–2754.e31 (2018).
54. J. R. Mazzulli, F. Zunke, O. Isacson, L. Studer, D. Krainc, α-Synuclein-induced lysosomal dysfunction occurs through disruptions in protein trafficking in human midbrain synucleinopathy models. *Proc. Natl. Acad. Sci. U.S.A.* **113**, 1931–1936 (2016).
55. R. Nehme *et al*., Combining NGN2 programming with developmental patterning generates human excitatory neurons with NMDAR-mediated synaptic transmission. *Cell Rep.* **23**, 2509–2523 (2018).
56. T. Imberdis, S. Fanning, A. Newman, N. Ramalingam, U. Dettmer, Studying α-Synuclein conformation by intact-cell cross-linking. *Methods Mol. Biol.* **1948**, 77–91 (2019).